CO 2 capture and sequestration in stable Ca-oxalate, via Ca-ascorbate promoted green reaction

Science of the Total Environment yyyy (2019) xxxx

??Contents lists available at ScienceDirect

Science of the Total Environment

journal homepage: www.elsevier.com/locate/scitotenv

CO_2 capture and sequestration in stable Ca-oxalate, *via* Ca-ascorbate promoted green reaction

Linda Pastero [a,*], Nadia Curetti [a], Marco Aldo Ortenzi [b], Marco Schiavoni [b], Enrico Destefanis [a], Alessandro Pavese [a]

[a] Department of Earth Sciences, University of Torino, Via Valperga Caluso, 35, 10125 Torino, Italy
[b] Department of Chemistry, University of Milan, Via Golgi 19, 20133 Milano, Italy

HIGHLIGHTS

- The increase of the amount of atmospheric CO_2 is still an unsolved issue.
- We handled the issue resorting to a multidisciplinary approach.
- We converted CO_2 into oxalate by using vitamin C as a sacrificial reductant.
- Calcium oxalates doubled the reaction performance compared to carbonate trapping.
- The conversion reaction was studied to improve its performance.

GRAPHICAL ABSTRACT

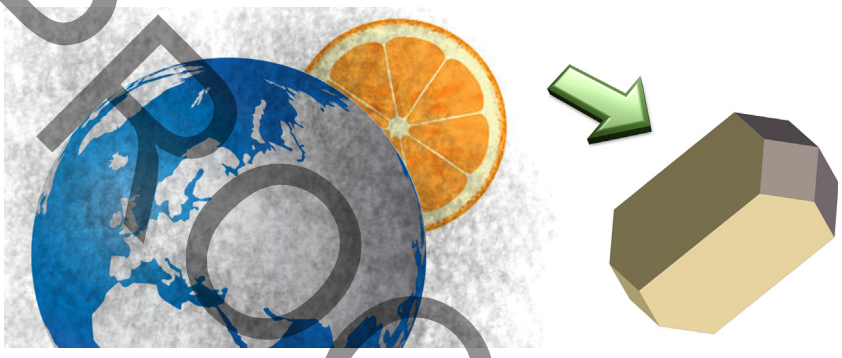

ARTICLE INFO

Article history:
Received 19 November 2018
Received in revised form 7 February 2019
Accepted 7 February 2019

Editor: Pavlos Kassomenos

Keywords:
Carbon dioxide
Sequestration
Calcium oxalate
Weddellite
Ascorbic acid
Calcium ascorbate

ABSTRACT

The increase in the amount of carbon dioxide (CO_2) emissions related to many anthropic activities is a persistent and growing problem. During the last years, many solutions have been set out, none of them being the ultimate one. Investigators agree on the need of a synergic approach to the problem, in terms of many complementary methods of sequestration that, combined with the reduction of production, will be able to decrease the concentration of the CO_2 in the atmosphere. In this work, we explore the use of a green reaction to trap the CO_2 into a stable crystalline phase (weddellite) resorting to a multidisciplinary approach. CO_2 is reduced and precipitated as calcium oxalate through vitamin C as a sacrificial reductant. Calcium oxalate crystals obtained show a startling good quality that increases their already great stability over a wide chemical and physical conditions' range.

1. Introduction

The alarms about the increase of the concentration of carbon dioxide in the atmosphere boosted the research in the field of the capture, sequestration and storage of carbon dioxide over the last decade. The environmental sustainability of anthropic activities involving the

* Corresponding author.
E-mail address: linda.pastero@unito.it (L. Pastero).

https://doi.org/10.1016/j.scitotenv.2019.02.114

production of CO_2 requires the reduction of the emissions in the atmosphere, the separation of CO_2 at the source (mainly power plants) and its transportation to the storage facilities. A single storage technology does not guarantee the necessary reduction of the emissions in the atmosphere. For that reason, many synergic technologies are needed. Presently, one of the most common storage method involves the injection of carbon dioxide into depleted oil, gas or carbon geological deposits. A chemical method of trapping is the mineral carbonation, *i.e.* the precipitation of carbonates from CO_2 in the presence of alkali oxides under favorable chemical and physical conditions.

A substantial part of the literature deals with the possibility of trapping and convert CO_2 into target commodities. This, in turn, leads to an increase in the interest in catalytical and photo-electrochemical reduction of CO_2. In fact, the surplus of CO_2 plays a role as a feedstock for the production of organic compounds, for instance, liquid fuels like methanol and dimethylether, formic acid or oxalic acid. The catalytic conversion of CO_2 into liquid fuels takes a major part in literature. Such a reaction occurs through an electrochemical reduction of CO_2 *via* homogeneous and heterogeneous catalysis, triggered by single catalysts or catalyst panels (Amatore and Saveant, 1981; Benson et al., 2009; Bockris and Wass, 1989; Costentin et al., 2013; Finn et al., 2012; Kortlever et al., 2015; Qiao et al., 2014; Qu and Duan, 2013; Rosen et al., 2011; Savéant, 2008; Schneider et al., 2012; Tryk et al., 2001; Whipple and Kenis, 2010).

A particular attention has been paid to the application of transition metal complexes to the reduction of carbon dioxide, and several molecular studies on the reactivity of carbon dioxide in the presence of such complexes have been published since the late sixties (Aresta et al., 1975; Darensbourg et al., 1981; Paik et al., 1969). From literature, the presence of transition-metal complexes appears mandatory to direct the reactivity of the $CO_2^{\bullet-}$ radical anion, *i.e.* a transient intermediate, towards a specific reaction product. Besides, electrochemical parameters, such as current density, have to be taken into due account and properly optimized.

Photo-electrochemical and catalytical reduction of CO_2 are associated to a significant energy drawback, but electrochemical reactions involve an inner-sphere electron transfer mechanism which is expected to result in lower activation energy with respect to redox catalysis that implies outer-sphere electron transfer (Savéant, 2008). In this context, the reduction of CO_2 to form oxalate has been accomplished by electrochemical reactions involving transition metal (Hg, Pb, Cu, Pd, Ag) complexes or anion radicals of aromatic hydrocarbons, esters, and nitriles (Amatore and Saveant, 1981; Angamuthu et al., 2010; Kushi et al., 1995; Savéant, 2008).

Transition metal complexes and hydroxides may allow the conversion of carbon dioxide into carbonate salts (van Albada et al., 2002; Youngme et al., 2001), as well.

Furthermore, glycol-amine mixtures and coordination complexes of polyamines have been reported to bind CO_2 reversibly through the formation of carbamates (García-España et al., 2004; Notni et al., 2008; Verdejo et al., 2006).

At the best of our knowledge, only a few authors proposed the reduction of CO_2 into $C_2O_4^{2-}$ to directly precipitate oxalates, ever recurring to metalorganic complexes (Angamuthu et al., 2010). In fact, the selective production of oxalate through the electrochemical reduction of CO_2 without resorting to catalysis, is thermodynamically unlikely due to the negative redox potential (some Authors reported a value of −2.21 V with respect to SCE in DMF (Amatore and Saveant, 1981)). For this reason, the conversion of CO_2 into $C_2O_4^{2-}$ has usually been achieved in the presence of metalorganic complexes or metal-sulfide clusters (Kushi et al., 1995).

The standard redox potential for the CO_2 reduction reaction into oxalic acid (Eq. (1)) in water at pH = 0 is −0.475 V (Bard et al., 1985; Kushi et al., 1995; Latimer, 1952).

$$2CO_2 + 2H^+ + 2e \rightarrow H_2C_2O_4 \quad (1)$$

In the present paper we assess the feasibility of the reaction of direct precipitation of calcium oxalates by carbon reduction without involving harmful reagents, transition-metal complexes or applying bias or current, but using calcium L-ascorbate in aqueous solution as reducing agent. We pay attention in particular to: i) Ca-oxalate precipitation reaction; ii) stability of the CO_2-storage system, *i.e.* crystal quality, size, morphology and forms development of the resulting Ca-oxalate crystals, iii) nature of the organic products from the degradation chain of the Ca-ascorbate. The quantification of the reaction kinetics and yield will be discussed in a further paper.

Ascorbic acid (AA) is a nontoxic and cost-effective reducing agent typically applied for biomedical purposes, food industry and geochemistry of soils. Additionally, L-ascorbic acid has been sometimes used as a sacrificial reductant in CO_2 reduction systems, in the presence of a chromophore, pyridine and using visible light at 470 ± 20 nm as a physical trigger (Izumi et al., 2010; Seshadri et al., 1994; Shah et al., 2018), or as a reducing agent for the reduction of graphene oxide dispersed in water at room temperature (Zhang et al., 2010).

As a sacrificial reductant, AA undergoes degradation. The degradation of AA has been studied by several Authors, dealing mainly with food industry, due to its applications as an antioxidant agent to extend the shelf life of foodstuff, and biomedical field, as a nutritional supplement.

AA is quite unstable in solution, its oxidation leading easily to the production of dehydroascorbic acid (DHA). Under acid conditions and in high ionic strength solutions, the dissociation degree decreases (Markarian and Sargsyan, 2011). The multiple steps of the degradation cascade are the subject of a huge number of publications. Leaving aside the details of the reactions, the degradation of ascorbate follows different pathways depending on the presence of enzymes and on the oxidative or non-oxidative conditions (Green and Fry, 2005; Kurata et al., 1967; Kurata and Sakurai, 1967; Parsons and Fry, 2010). DHA, in turn, transforms non-enzymatically into a variety of degradation products (ascorbate cascade) and gives rise to a very unstable in solution, easily delactonized to diketogulonic acid (DKG) and further degradation products. Moreover, it has been demonstrated by Koshiishi et al. (1998) that the CO_2-H_2CO_3-$NaHCO_3$ buffer participates in the hydrolysis of DHA in plasma and Dulbecco's modified Eagle's medium. The final degradation product reported in the literature is oxalic acid.

Nearly all the papers reporting the presence of oxalic acid at the end of the reaction cascade deal with *in vivo* experiments.

The standard redox potential of the oxidation of AA into DHA (Eq. (2)) has been found to be strongly pH-dependent, the redox properties being modified by the proton availability (Bode and Rose, 1990; Lovander et al., 2018).

$$AA \rightarrow DHA + 2H^+ + 2e \quad (2)$$

Many values of the standard redox potential have been experimentally determined and reported in the literature, ranging from 0.066 V (Borsook and Keighley, 1933) to 0.4 V (Bartlett and Wallace, 1999; Lovander et al., 2018). Matsui and coworkers (Matsui et al., 2015) calculated the standard redox potentials of vitamin C, NAD and NADH, obtaining a value of 0.5 V and confirming the earlier experimental values present in literature.

In order to precipitate a crystalline phase, we used calcium L-ascorbate as the reducing agent to promote the precipitation of the nearly insoluble ($K_{sp}^{COM} = 2.32 \times 10^{-9}$ (Lide, 2003)) calcium oxalate, *i.e.* CaC_2O_4. Calcium oxalate crystallizes as monohydrate (COM, whewellite, $P2_1/c$; $a = 6.290(1)$, $b = 14.583(1)$, $c = 10.116(1)$ Å, $\beta = 109.46(2)°$ (Tazzoli and Domeneghetti, 1980)), dihydrate (COD, weddellite, $I4/m$, $a = 12.371(3)$, $c = 7.357(1)$ Å (Tazzoli and Domeneghetti, 1980)) or trihydrate (COT, caoxite, $P\bar{1}$; $a = 6.1097(13)$ Å, $b = 7.1642(10)$ Å, $c = 8.4422(17)$ Å, $\alpha = 76.43(1)$, $\beta = 70.19(2)$, $\gamma = 70.91(2)$ (Conti et al., 2015)). Caoxite and weddellite are considered as the metastable crystalline forms of calcium oxalate and tend to dehydrate (by time or heating) into whewellite (Bretherton and

Rodgers, 1998; Conti et al., 2010, 2015; Izatulina et al., 2018; Ouyang et al., 2006).

Calcium oxalates are the sound topic of many biomedical papers devoted to pathological mineralization *in vivo*. Daudon (2015) and Daudon and Frochot (2015) presented some interesting review papers about crystalluria, emphasizing the effect of pH on the selection of the hydration state, on the modification of the crystal morphology and the stability of calcium oxalate along with pH variations. Oxalates play an important role in the geochemistry of soils and plants, especially cactacee (Graustein et al., 1977; Hartl et al., 2007; Monje and Baran, 2002). In 2006, Garvie stressed the hypothesis of a complex biochemical reaction pathway that allows Saguaro cactus to convert atmospheric CO_2 into oxalates (Garvie, 2006).

The experimental setup and related reaction chains are here discussed to obtain selectively well-crystallized weddellite (COD) from a solution using CO_2 as a source of carbon, and calcium L-ascorbate as a reducing agent and calcium reservoir. Due to the generally low pH values of the solutions all over the experiments, no competition between calcium oxalates and calcium carbonates is expected, as confirmed by the phase composition of the products. Moreover, the low pH provides equilibrium conditions expressed *via* the first dissociation constant of ascorbic acid, associated with the redox potential values mentioned above.

2. Materials and methods

All reagents were analytical grade from Sigma-Aldrich. Pure CO_2 and N_2 were purchased from Sapio. Ultrapure water (18 MΩ) was obtained by using an Elga Purelab Flex3 ultrapure water system. The CO_2-trapping system's performance was tested by different experimental setups, namely A, G, B and DB.

The **A** setup was used in preliminary experiments to test our hypothesis and precipitate calcium oxalate from the reduction of CO_2 in air. A calcium L-ascorbate 1 M solution, in a vessel, was allowed to react at open-air conditions.

The **G** setup was used for a series of experiments meant to globally provide a "proof of concept". Multi-well cell culture plates (six wells in a plate) were chosen as reactors to i) confirm the reliability of the method and ii) qualitatively estimate the effect of the concentration of the solution on the precipitate (quality and size of crystals, crystal phase selection). Each well was filled with 5 mL of $CaC_{12}H_{14}O_{12}$ solution (CaAsc hereinafter) 1 M. Given that the G experiments yield preliminary information, the concentration of the ascorbic acid was chosen high (1 M or 0.1 M) to maximize its effect. One well was filled with $(NH_4)_2CO_3$ solution with concentration 0.1 M or 0.01 M as a source of carbon dioxide, allowing the slow diffusion of gases released by the thermal decomposition of ammonium carbonate (Gómez-Morales et al., 2010; Lakshminarayanan et al., 2002; Pastero and Aquilano, 2018). Starting pH ranged between 2.5 and 3. The multi-well plate was sealed to ensure the saturation of the inner volume in CO_2. The value of the final pH was measured at the end of the experiments, giving figures that range between 3 and 3.5. Details of the experiments are reported in Table SI1.

The **B** experiments were carried out in a glass reactor filled with 1 L of 1 M CaAsc solution. CaAsc solution was prepared by previously degassed ultrapure water, bubbling N_2 into the solution and under N_2 atmosphere, to avoid the contact of the solution with the CO_2 prior to the beginning of the experiment. Carbon dioxide was bubbled into the solution, the flux rate being kept constant at 300 mL/min under continuous stirring.

BD experiments' setup was close to B's. The reaction performance was improved by increasing the surface/volume ratio of the solution using a proportioning pump to efficiently mix CO_2 with the solution. In this way, we obtained a bubble-drop system reacting since the initial stages of the experiment, each droplet acting as a microfluidic reactor. Moreover, the residual solution was recirculated after filtration to recover the unreacted solution without loss. A scheme of the BD experimental setup is reported in Fig. SI1.

A Zeiss Axiolab Pol polarized microscope (Carl Zeiss AG, Germany) equipped with a rotary stage and a JVC 3-CCD KY F55B camera with 750 lines of horizontal resolution and a 60 dB signal-to-noise ratio was used for the optical observations.

Scanning Electron Microsopy (SEM) imaging was performed using a JSM IT300LV High Vacuum – Low Vacuum 10/650 Pa - 0.3–30 kV (JEOL USA Inc.) equipped with secondary electron (SE) and backscattered electron (BSE) detectors (typical experimental conditions: W filament, EHT 20 kV, working distance 5 mm).

Powder X-ray Diffraction (PXRD) measurements for the raw identification of the crystalline phases were carried out by a Siemens D5000 diffractometer (Bragg-Brentano geometry, $2.5° < 2\theta < 100°$, step size 0.01, 1 s/step scan time; operating at 40 kV and 30 mA).

High Perfomance Liquid Chromatography (HPLC) analyses were performed using a Jasco PU-4180 pump and a Photo Diode Array Detector Jasco MD-4015 equipped with a Phenomenex Synergi® 4 μm hydro-RP 80 Å HPLC Column 250 * 4.6 mm. The mobile phase was either water + 0.1% Acetic Acid (phase A) or acetonitrile (phase B). All samples were diluted to achieve a concentration of 1–2 mg/mL. The analyses were carried out using the gradients reported in Table 1:

Single crystal X-ray diffraction measurements were performed on several single crystals of COD (a synthetic analog of weddellite), sorted on the basis of their optical features, and preliminary diffraction tests were performed to check the crystallinity grade of their structures. Full X-ray single crystal diffraction experiments were carried out at room conditions on two crystals (CaOX-A-1 and G13-3) coming from as many syntheses, with a Gemini R-Ultra X-ray diffractometer equipped with a Ruby CCD detector, using monochromatic CuKα radiation and the tube operating at 50 kV and 40 mA (CrisDi Interdepartmental Center, University of Torino). The 171.37.35 version of CrysAlysPro software (Rigaku Technologies) was used to integrate the intensity data and for analytical absorption and Lorentz-polarization correction.

Electrochemical measurement were performed using both a Thermo Orion 4 Star Benchtop Multiparameter Meter equipped with an Orion 9778BNWP Combination Redox/ORP (Oxidation Reduction Potential) Electrode and an Orion 013005MD DuraProbe 4-Electrode Conductivity Cell Probe and an Orion 420A Benchtop pH/mV/temperature Meter equipped with an Orion 9156SC Combination pH Electrode.

Free calcium in solution was measured by complexometric titration with a solution 0.02 M of EDTA and calconcarbonic acid as an indicator.

Single points of measurements of the electrochemical parameters and free calcium concentration were carried out as snapshots of the systems' behavior on all the experiments referred to B and BD setup (see Table SI2). A systematic collection of the electrochemical and chemical information was performed on B03 and B12 experiments to compare the performance of the two setups.

3. Results and discussion

3.1. Oxalate precipitation

All the experiments involve the precipitation of crystalline calcium oxalate, and the reaction yield markedly depends on the reaction surface exposed to CO_2. PXRD measurements confirmed the presence of

Table ??1??
Gradients used for HPLC analyses.

Time	Phase A (%)	Phase B (%)
0	100	0
3	99	1
9.4	95	5
11	50	50
12.5	95	5
13.5	99	1

weddellite, sometimes associated to whewellite as a byproduct (Table SI1).

Preliminary A and G experiments involved the precipitation of Ca-oxalate in slowed down systems because of the experimental set-up. In fact, the diffusion rate of CO_2 through the interface between gas and solution in the reacting volume and the comparatively small exchange area (open surface of the vessel) reduced the rate of conversion of carbon dioxide into oxalate. Consequently, the nucleation rate of oxalates in the reaction vessel is low and not uniformly distributed through the volume because of the CO_2 gradient from the surface towards the bulk of the solution. In A experiments, many nucleation events have been recognized from the size distribution of the crystals. A few large crystals useful for single crystal X-ray measurements are precipitated, as well.

On the contrary, in G experiments the size distribution of the crystals is quite uniform, varying with the experimental conditions. The size distribution in the experiment G4 is given as an example in Fig. 1. This behavior is due to the occurrence of a unique nucleation event, the nucleation frequency and the crystal size both depending on the supersaturation of the system with respect to weddellite. Moreover, even in presence of basic species, the pH of the solution lies out of the stability field of the carbonate, thus avoiding the competition between carbonates and oxalates during precipitation.

From A and G experiments we obtained a few suggestions about the effect of the chemical conditions on the precipitation of calcium oxalates. No correlation between the major chemical parameters of the solution and the crystal phases obtained can be found out (Table SI1). Crystallization takes place after a few hours of exposure to the selected atmosphere, depending on the concentration of the CO_2 (obviously slower in A than in G experiments, where CO_2 is pumped in from the solution of ammonium carbonate). The main phase obtained is weddellite, as PXRD measurements (Fig. 2) confirmed. Whewellite is sometimes found as a byproduct of the reaction, its signal in PXRD patterns being nearly undetectable.

Additionally, it must be kept in mind that the crystallization behavior in A setup is the result of the cooperative oxidative process driven by both CO_2 and O_2 from air, while in G, B and BD setups the system is kept free of oxygen to confirm the effect of the carbon dioxide.

Weddellite is the prevailing phase in all long-lasting experiments (Fig. 3a and b, Table SI1), while whewellite may be obtained sometimes (Fig. 3c and d), mainly in short time experiments. The appearance of whewellite is a reaction kinetics effect related to the supersaturation of the system according to Brown and coworkers (Brown et al., 1989), meaning that at high supersaturation (*i.e.* during the early stages of the precipitation event) both weddellite and whewellite are precipitated. On the contrary, in *in vivo* experiments, (Daudon, 2015; Daudon and Frochot, 2015), a strong dependence of the phase precipitated on the pH is recognized.

The flat (F) bipyramid {101} rules the morphology of weddellite in all our experiments. Keeping as a reference for indexing the F {101} bipyramid, the prisms {100}, {110} or {120} are found stable, depending on the experimental conditions. In A and G experiments, only the {100} prism has been observed, its appearance depending rather on the nucleation rate imposed to the system than on the chemical conditions of the system: if the nucleation rate is low and, consequently, the system behavior is dominated by the growth, the morphological importance of the prism increases. On the other hand, in experiments B and BD, where CO_2 is bubbled into the system, a habit modification sequence can be observed, involving the appearance of several prisms: from {100} to {120} to {110}, while the {101} bipyramid occurs as a stable crystal form since the early stages of growth.

It is quite interesting to observe that the morphology of the smaller crystals (around 20 μm long) is made up by the association of {101} + {120} forms, whereas the larger crystals show the association of {101} + {110} forms. In Fig. 4a, a twirling effect of the macrosteps on the {101} around the four-fold axis can be recognized. The twirling is a kinetic effect related to the stabilization of the {110} prism instead of the {120} one, changing the growth conditions during time.

According to the PBC's analysis of the structure of the weddellite performed by Franchini-Angela and Aquilano (1979) and Heijnen and Van Duijneveldt (1984), the {110}, {100} and {101} forms show a F (flat) character. The profile of the {120}-prism can be described as an S (stepped) form originated from the composition of {100} and {110}-F segments (Supporting Information, Fig. SI2), the stabilization of either leading to the two "morphological end-members" shown in Fig. SI2(a and c) and experimentally obtained, as a function of the growth conditions. The complex morphological behavior of weddellite crystals is beyond the purpose of this work. Nevertheless, it is important to stress that the main forms appearing in the crystals obtained by CO_2 trapping show an F-character, associated to highly stable faces. The nature of the surfaces exposed to the surroundings contributes, along with the quality of the bulk structure, points to the high overall stability of the crystals.

Whewellite usually grows as tabular crystals frequently twinned and dominated by the pinacoid {010} encompassed by rounded edges belonging to the 2-fold axis zone (Fig. 3c and d).

Weddellite was the only phase obtained from long-lasting B and BD experiments, as confirmed by the PXRD measurements. In B and BD experiments, continuous electrochemical measurements (pH, ORP, conductivity, and Ca^{++} concentration) have been performed to observe the kinetics of the precipitation of calcium oxalates. The measurements were affected by strong matrix effects and instrumental drift, so we resorted to discontinuous measurements to avoid instrumental drift (Fig. 5). For the sake of brevity, the data from experiments B03 and BD01, only, will be reported below (see Supporting Information

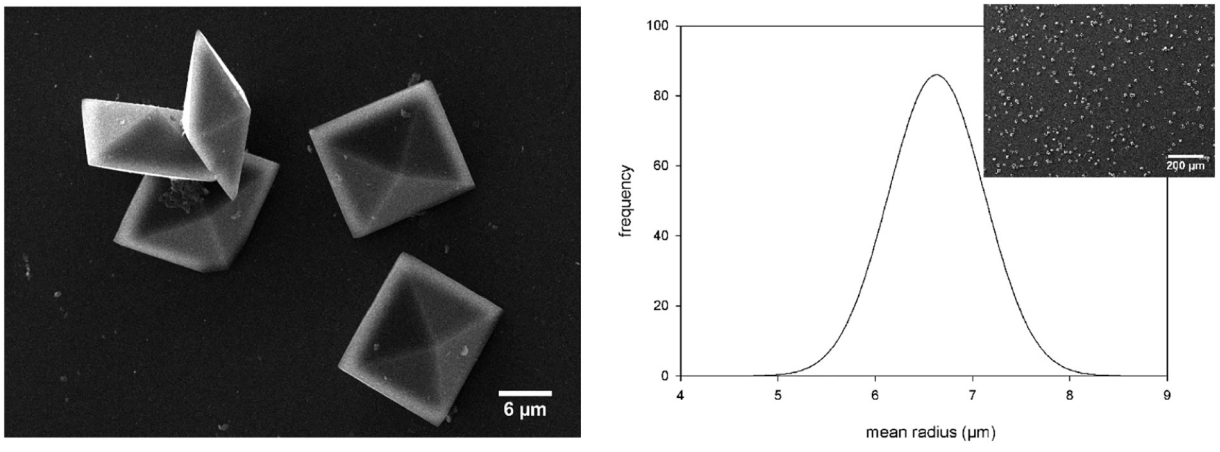

Fig. 1. Size distribution of the weddellite crystals obtained from the experiment G4.

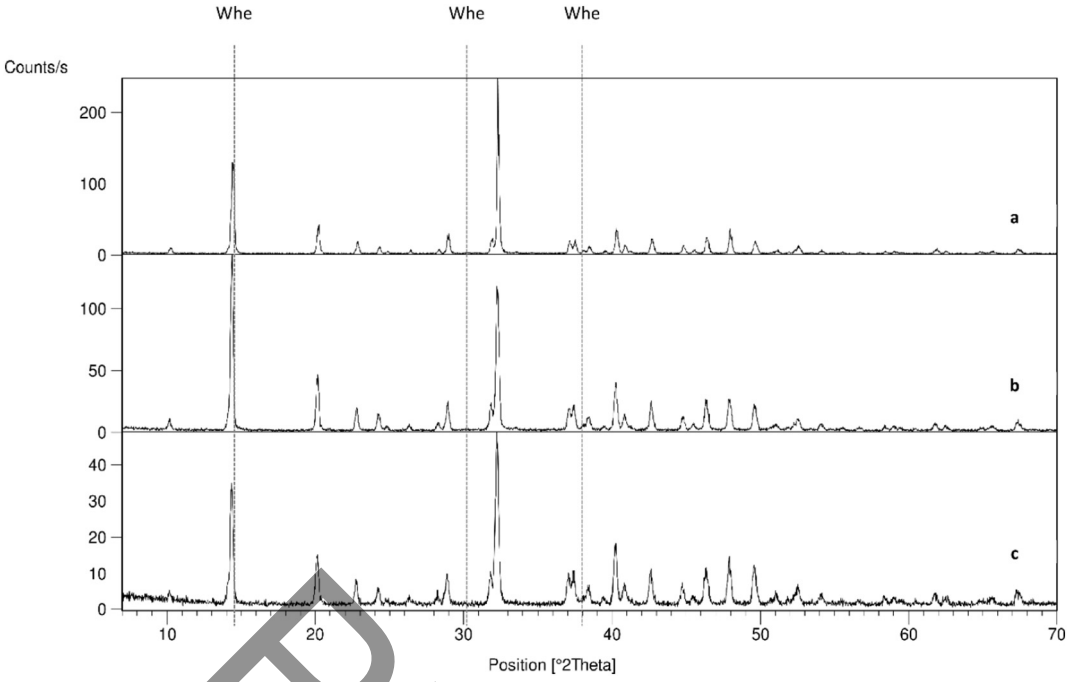

Fig. 2. PXRD data collections of the crystallization products of three illustrative experiments. a) G setup, b) BD setup and c) 24 h long A setup patterns. In a) and b), the weak signal from whewellite is detected while in c diffraction pattern only weddellite is found.

Table SI2). Both the experiments underwent to a stop of the CO_2 supply from 2.5 to 191 h in the case of the experiment BD01 and from 12 to 170 h in the case of the experiment B03. During the stop of the gas supply, the systems were left to react with the CO_2 stored into the upper part of the reactors to stress the effect of the increased reactive surface in BD experiments.

The ORP measurements were subjected to sharp fluctuations, with scattered values ranging from −60 to +40 mV. For this reason, we did not consider reliable ORP measurements (not reported).

The pH value (Fig. 5a) shows a constant decreasing trend in both B (white diamonds) and BD (black triangles) experiments, the slope being higher in B setup than BD. It must be considered that the CaAsc

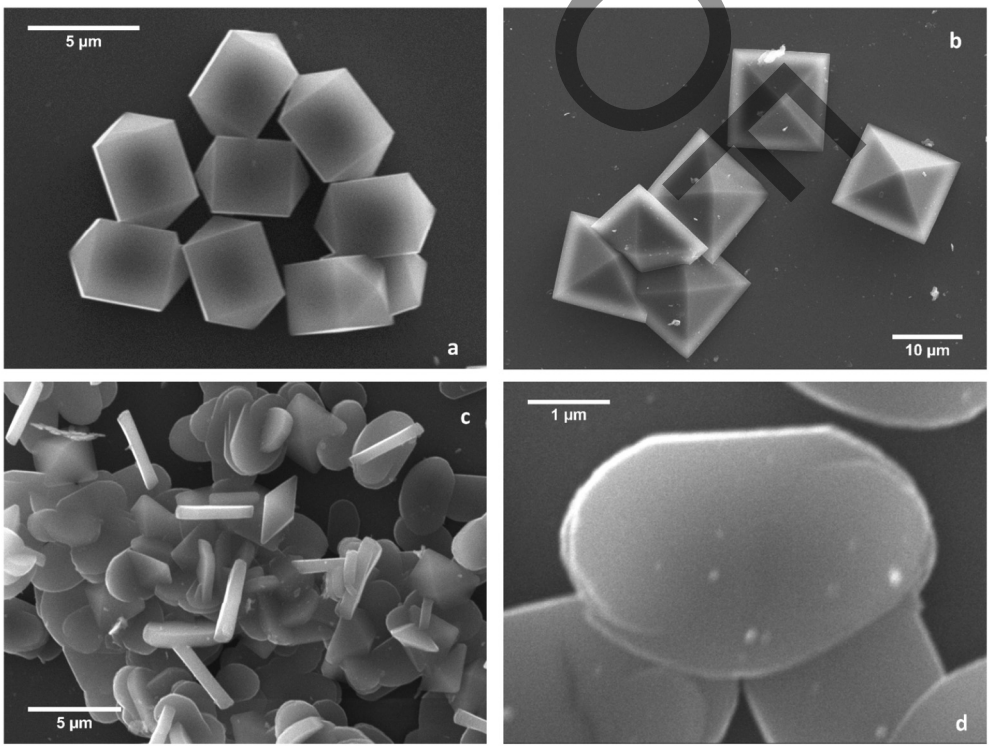

Fig. 3. Weddellite (a and b) and whewellite (c and d) obtained from experiments G. The morphology of weddellite is dominated by the ever-present {101} bipyramid. The extension of the prism {100} depends on the rate of nucleation and growth. Whewellite usually shows an incomplete growth morphology, dominated by the {010} pinacoid and usually twinned (d). The facetes surrounding the {010} pinacoid are not differentiated.

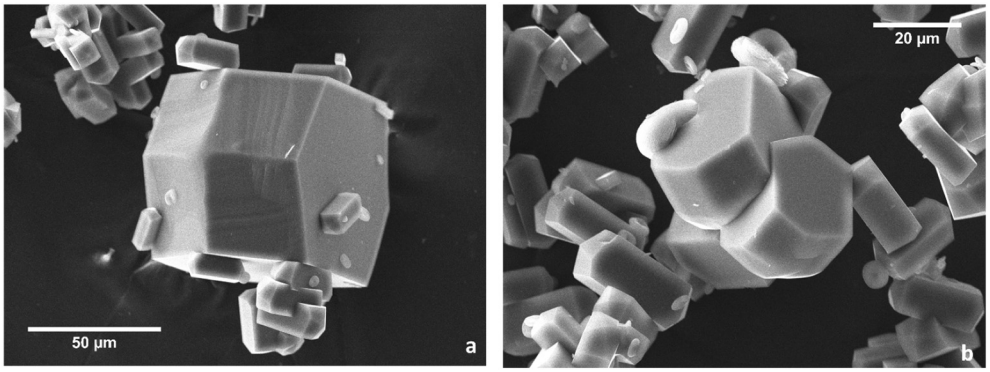

Fig. 4. In a) and b) at least two generations of weddellite crystals are recognizable, the first (larger) showing the {101} + {110} association of forms and the second (smaller, around 20 μm) showing the {101} + {120} association of forms. Moreover, the large crystal belonging to the first generation shows a twirling of the macrosteps on the surface of the pyramid indicating the evolution of the growth habit.

solution is a weak buffer, able to compensate the slight acidification induced by the carbonic acid generated by bubbling the CO_2 only to a certain extent. The higher slope of the pH trend in the B system probably depends on the increase of the concentration of the CO_2 dissolved and still unreacted. In fact, due to the experimental setup of the B system, a flux of 300 mL/min of CO_2 is injected into the CaAsc solution under continuous stirring. CO_2 bubbles forming at the gas inlet quickly reach the interface between the CaAsc solution and the CO_2 saturated atmosphere inside the vessel, even under stirring. Furthermore, the CO_2 does not dissolve readily in acidic conditions. So, the time of contact between the bubble surface and the solution is quite short, and the redox reaction almost totally occurs at the interface between the reactor's atmosphere and the solution. For such reasons, the system kinetics can be considered pretty slow and comparable to that of the A and G experiments, driven by the diffusion of the CO_2 from the solution/atmosphere interface towards the bulk of the solution. On the contrary, in

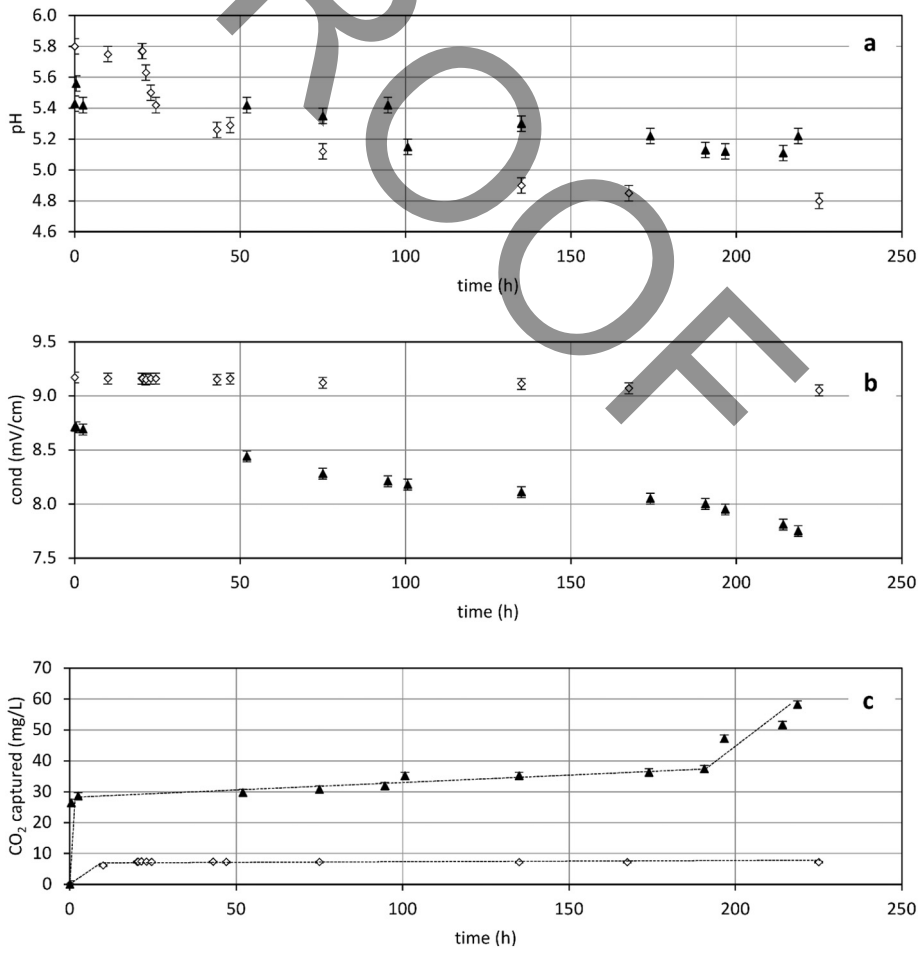

Fig. 5. White diamonds: B setup; black triangles: BD setup. a) pH trend during 225 h of experiment, quite similar for both the experimental setups, showing a higher slope in BD setup; b) conductivity values follow a pretty different pathway in B and BD experiments: in BD setup, the decrease is strongly marked while in B experiments the slope is gentle, meaning that the subtraction of solute species in BD setup is more efficient with respect to B setup; c) mg/L of CO_2 precipitated as calcium oxalate: in BD experiments as the conductivity quickly decreases, the amount of captured CO_2 quickly increases whereas in B experiments it joins a plateau after a few hours.

Table ??2??
Fluxes of CO_2 injection and release, rate of equilibration of the CO_2 among liquid, gas and crystalline phase during the oxalate precipitation reaction as obtained from the model in Eq. (3) to the BD and B experiments in Fig. 5.

Experimental setup	Slope (ppm/h)	Φ_{in} (mol/h)	Φ_{out} (mol/h)	CO_2 trapping (mol/h)	CO_2 liquid/gas equilibration (mol/h)
BD setup	12	0.815	0.170	0.6	0.0454
	0.05 (plateau)	0	0	0.0025	−0.0025
	0.8	0.815	0.730	0.04	0.0454
B setup	0.6	0.815	0.740	0.03	0.740
	0 (plateau)	0	0	0	0

BD experiments, the bubble/drop setup increases the reactive surface of the solution and consequently the diffusion of the CO_2 in small volumes (droplets) of CaAsc solution.

An approximate estimate of the amount of reaction surface in BD setup compared to B has been performed considering the reactor's and pipes' sizes, the fluxes of fluids involved and the mean size of a solution droplet. The determined trend is reported in Fig. 7. At a first approximation, the increase of the reactive surface in a BD setup is about 50 times as large as the reactive surface in a B experiment, performed in the same reactor without using a partitioning pump. An increase of reaction surface in BD setup corresponds to an increase of the CO_2 reaction rate and, accordingly, of the concentration of oxalate ready for the precipitation in the form of its calcium salt. In BD setup the saturation with respect to calcium oxalate is reached faster in comparison to the B setup, and the CO_2 is swiftly subtracted from the system, allowing the weak buffer to operate slowing down the decrease of the pH value.

The conductivity (Fig. 5b) diminishes in both systems, but the decrease in BD setup is faster than in B setup for the mechanisms just described: to a higher precipitation rate of calcium oxalate corresponds a faster subtraction of the dissolved species, related to the higher slope in the conductivity decrease in BD setup.

The subtraction of calcium as a dissolved species in solution corresponds to the precipitation of calcium oxalate. We used the concentration of free calcium in solution to indirectly evaluate the performance of the system regarding the amount of CO_2 precipitated into calcium oxalate (Fig. 5c).

In B setup (Fig. 5c, white diamonds), the amount of CO_2 captured increases during the first 12 h of reaction, with a 0.6 ppm/h slope that represents the rate of CO_2 capture. After this time of reaction, the CO_2 supply is stopped and the system reaches a 0 ppm/h slope plateau, meaning that no more CO_2 is reduced to $C_2O_4^{2-}$. Thus, the B system based on a limited exchange interface (free surface) between gas and solution inside the reactor, comes to a complete failure, suggesting that the simple mechanism of bubbling of carbon dioxide into a stirred calcium ascorbate solution is far from being performant. The system fails because of the equilibration between gaseous carbon dioxide in the free volume of the reactor, which diffuses from the interface towards the volume of the CaAsc solution, and total CO_2 dissolved into the solution. Experimentally we recovered 152 mg/L of calcium oxalate, a little less with respect to that calculated from free calcium concentration (160 mg/L, corresponding to 86 mg/L of CO_2).

In BD setup (Fig. 5c, black triangles), the trend in CO_2 sequestration is deeply modified, undergoing a sudden increase during the first 2.5 h, with a mean capture rate of about 12 ppm/h (c.a 37 ppm/h during the first 40 min that decreases to 1 ppm/h during the next 2 h) that reasonably represents the effect of the combination of both BD and B setups on a fresh CaAsc solution. After the early 2.5 h, the CO_2 supply is stopped and the system shows a severe downturn of the capture rate, with a slope of 0.05 ppm/h that continues until the CO_2 flux is restored. This behavior is comparable with the plateau reached in B setup already described. During this time, the system tends to equilibrate the gaseous CO_2 in the free volume of the vessel with the CO_2 dissolved into the solution, the whole volume of the solution being characterized by a decreasing downward gradient of CO_2 from the interface with the saturated atmosphere towards the bulk of the volume because of the diffusion that proceeds from the interface. The very slow reaction rate likely depends on the equilibration of the gas between the free volume of the vessel and solution. When the flux of CO_2 is restored, the supersaturation increases suddenly and a new precipitation reaction occurs, with a capture rate that rises accordingly, with a slope of 0.7 ppm/h, comparable to that at the early stages of precipitation in both BD (1 ppm/h) and B (0.6 ppm/h) setups.

Summarizing, the BD setup is much more efficient than the B setup because of the larger reactive surface (50 times larger). This gives the system a first pulse of supersaturation that results in a very high starting precipitation rate (37 ppm/h). Then, the system slows down likely depending on the decrease in the efficiency of the reducing agent.

At the end of the experiment we recovered 515 mg/L of calcium oxalates, the calculated total amount being 835 mg/L (corresponding to 448 mg/L of CO_2). The marked difference is due to the precipitate that was not recovered from the pipes.

The rate of CO_2 capture can be roughly described by the following model (Eq. (3))

$$\Phi_{in} = \left(1 + k_{l/g}\right)\dot{n}_{CO_2\,g} + 2\dot{n}_{ox} + \Phi_{out} \tag{3}$$

Φ_{in} and Φ_{out} being respectively the flux of CO_2 injected into the reactor and the flux of residual (unreacted) CO_2, $k_{l/g}$ the partition coefficient

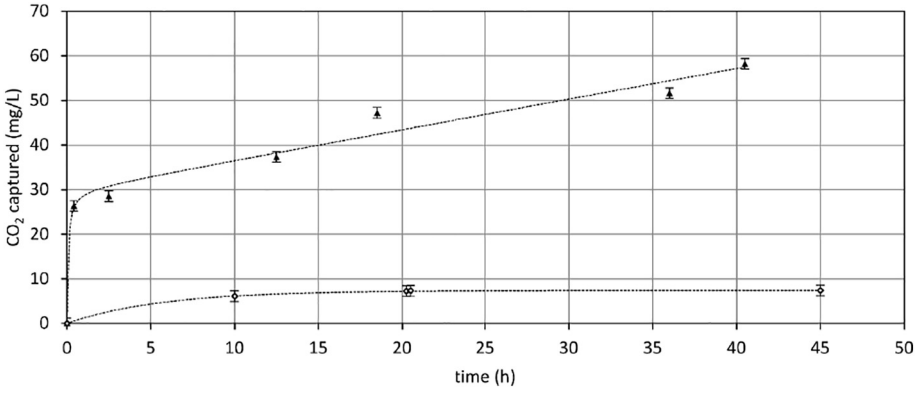

Fig. 6. White diamonds: B setup; black triangles: BD setup. Not considering the interruption of CO_2 supply, the CO_2 captured follows the trends reported. B setup reaches a real plateau after a few hours of reaction while BD setup still reacts. Moreover, the reaction yields after two days of reaction are dramatically different.

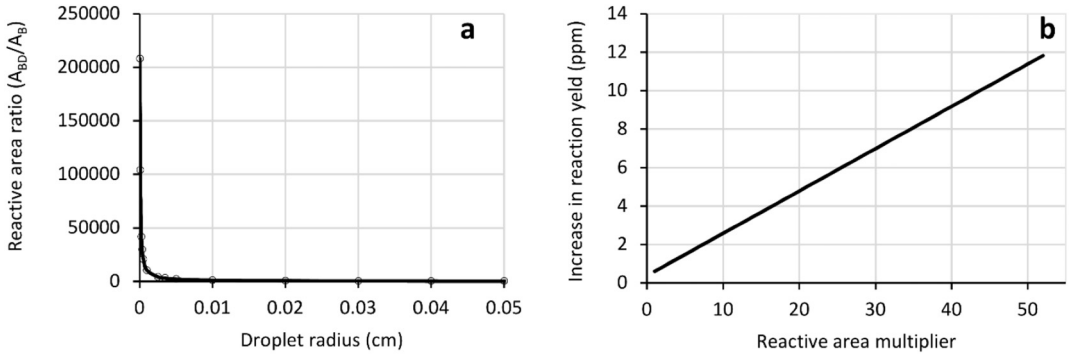

Fig. 7. a) Rough evaluation of the reactive area ratio (A_{BD}/A_B) *vs* droplet radius and b) of the increase in reaction yield increasing the reactive area.

of CO_2 between liquid and gas phase, $n_{CO2,\,g}$ the moles of CO_2 in the gas phase and finally n_{ox} the moles of oxalates precipitated by CO_2 reduction. In the operative conditions (partial pressure 100 kPa, temperature 20 °C, density 1.815 g/L) and approximating the saturation of the solution to the values tabulated for water, (molar fraction $\chi_{CO2l} = 7.04 \times 10^{-4}$ (Lide, 2003)), the partition coefficient $k_{l/g}$ can be approximated to $\chi_{CO2l}/\chi_{CO2g} = 7.04 \times 10^{-4}$.

When the flux of CO_2 injected into the reactor is constant, the reactor represents an open thermodynamic system: the CO_2 will distribute into the liquid and vapor phases as described by the partition coefficient $k_{l/g}$ and the oxalate precipitation will proceed as the system tends to equilibrate. At the equilibrium, the term $(1 + k_{l/g})\dot{n}_{CO_2,g}$ is a constant with a value depending on the partial pressure of the gas into the gas mixture, the temperature and the partition coefficient between gas and liquid. The rate of trapping of the CO_2 into the oxalate phase and the flux of CO_2 expelled from the reactor are therefore linked and finally dependent on the reducing power of the CaAsc.

Turning off the flux of CO_2, the thermodynamic system becomes closed and tends to equilibrate the CO_2 dissolved into the solution with that stored into the free volume of the reactor by precipitating the excess as calcium oxalate. Experimentally, this is represented in BD setup by the smooth ramp (0.05 ppm/h) and in B setup by the plateau at 0 ppm/h in Fig. 5c.

Based on these considerations, a rough evaluation of the rate of consumption of CO_2 from the gas phase, representing the CO_2 equilibration rate at a given flux and oxalate precipitation rate, is possible starting from the model proposed in Eq. (3). The results are reported in Table 2.

The rate of oxalate production will depend on the efficiency of the reducing agent, that decreases with aging. In fact, if considering the concentration of CO_2 trapped disregarding the supply interruption (Fig. 6), the strong trapping effect at the beginning (fresh reducing agent) decreases after the first 40 min from 37 ppm/h to a mean value of 0.7 ppm/h, according to the aging of the reducing agent. Anyway, the direct comparison between the B and BD systems disregarding the interruption of the CO_2 supply even more so brings to light the different behavior of the trapping and its dependence on the reactive surface. Besides the different capture rates shown at the beginning of the process, the main difference is stressed by the slope of the two graphs after the early stages of the experiment: BD setup shows a linear quite rapid increase unlike B setup, that undergoes to a complete breakdown.

The process of CO_2 trapping so far described can be divided into two steps:

i) the red-ox reaction involving CO_2 and CaAsc and leading to the formation of the oxalate in solution;
ii) the precipitation of the calcium oxalate.

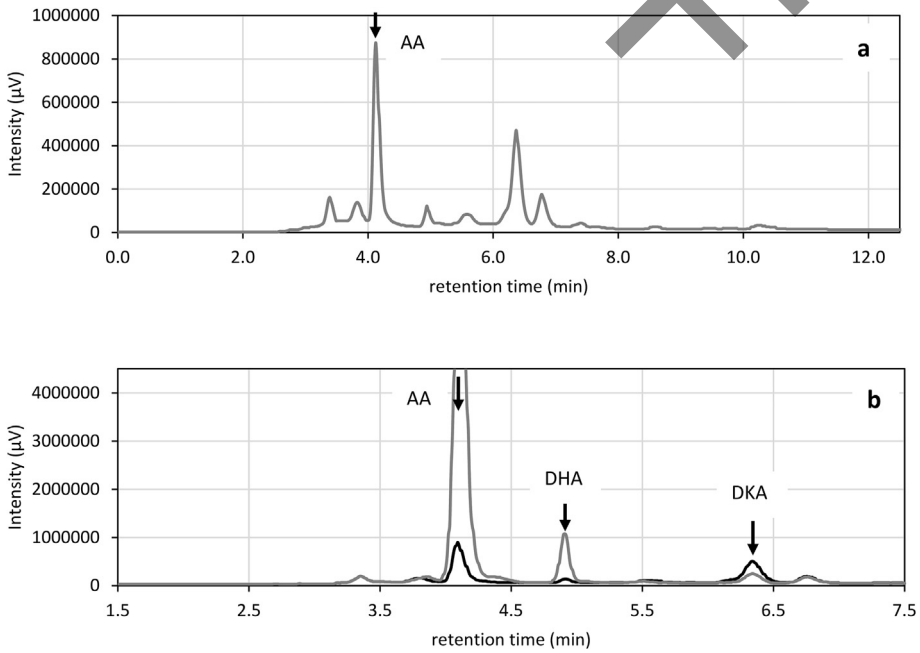

Fig. 8. HPLC spectra of the diluted AA-air sample showing the retention times of AA, DHA and DKA.

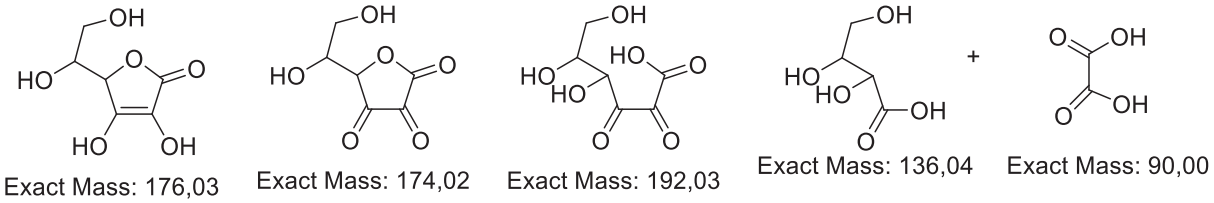

Scheme 1. Degradation products starting from Ascorbic acid at pH = 2.

The second step occurs only if the first step is on track, so the first one results to be the rate-determining reaction of the whole process. Once the process is in progress, it continues up to the exhaustion of the calcium reservoir or of the reducing capacity of the ascorbate ion. Once the process is triggered, the two reactions' rates are reciprocally independent and the precipitation reaction can be supposed to be very fast, because of the very low solubility of the crystalline phase.

In the light of the above, we are able to correlate the efficiency of the CO_2 capture system with the amount of solution' surface exposed to the gas: a large surface increases the efficiency of the capturing process. In fact, considering the first step of the reaction, the B setup shows a capture rate of 0.6 ppm/h, while the BD setup shows a mean capture rate of 12 ppm/h (37 ppm/h at the very beginning). As already stated, the reactive area is about 50 times larger in BD setup than in B setup. Assuming a linear dependence of the reaction yield *versus* reactive area, we can roughly predict that the reaction efficiency can be increased by a factor two by just increasing the exposed surface four times more.

Cross-referencing this evaluation with the dependence of the reactive area from the droplet size as calculated, we can predict that, for a 2.5 μm sized droplet in BD setup, the yield of the reaction considering the BD reaction rate of 12 ppm/h will be increased by 42 k times, leading to the precipitation of 27 g/L of weddellite, corresponding to 0.165 mol/L of weddellite. This foreseen yield is well-matched with the concentration of the CaAsc (1 M) used.

3.2. HPLC determinations

Since the degradation of ascorbic acid is a very complex sequence of reactions, as described at the beginning of this work, it was mandatory to verify if, under our experimental conditions, ascorbic acid leads to oxalic acid at the end of the transformation cascade. To do this, we performed HPLC analysis on AA and CaAsc samples stored in air (AA-air, CaAsc-air), to compare with samples stored under inert nitrogen atmosphere (CaAsc-N_2) avoiding any contact with CO_2.

AA-air sample (1 M) was diluted to enter the linearity range and the analysis was performed at 280 nm. The sample shows the presence of AA (peak at 4,1 min in Fig. 8a) and many decomposition products, the more polar being present at the beginning of the chromatogram and the less polar being eluted at higher times.

The decomposition pathway that was considered in the experimental condition used (*i.e.* pH = 2) involves the production of different species, according to Scheme 1.

The peak at 4.9 (Fig. 8a,b) minutes belongs to dehydroascorbic acid (DHA), showing a UV spectrum comparable to that of AA. Comparing the chromatogram at 250 nm (Fig. 8b, gray) with the one at 280 nm (Fig. 8b, black), AA and DHA are the only products with lower intensity at 280 nm. The peak at 6.4 min probably belongs to diketogulonic acid (DKA).

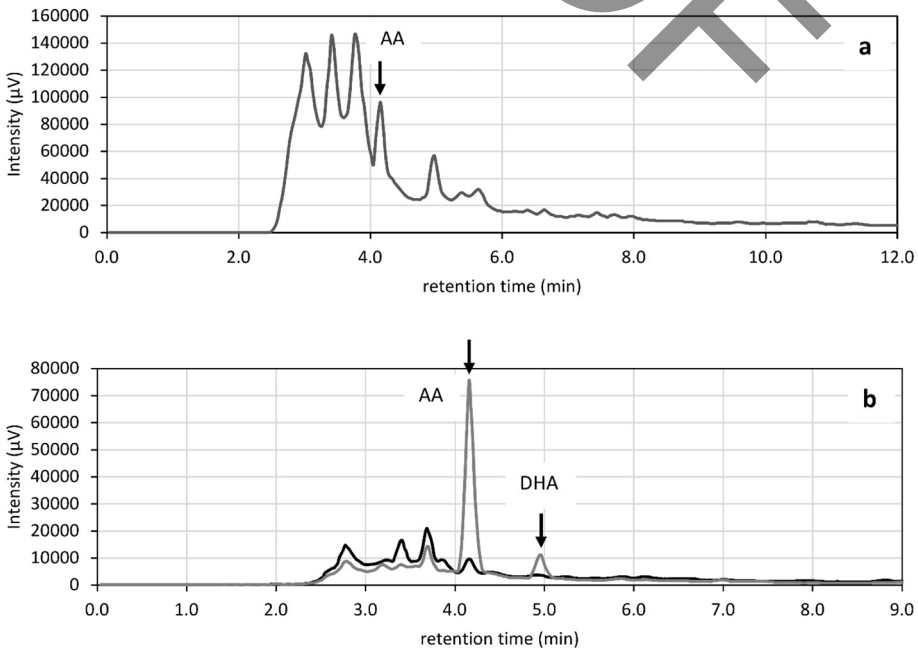

Fig. 9. HPLC spectra of the concentrated (9a) and diluted CaAsc-air sample (9b) showing the retention times of AA and DHA. Spectrum of concentrated CaAsc-air sample was obtained at 280 nm.

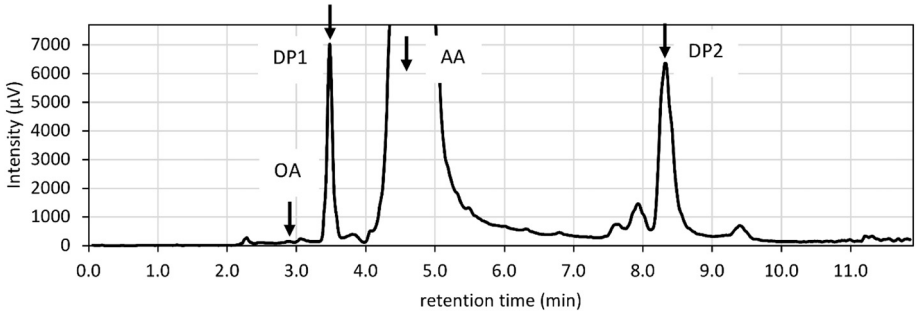

Fig. 10. HPLC spectrum of the diluted CaAsc-N_2 sample showing the retention times of AA, OA and two degradation products (DP1 and DP2).

As for AA, CaAsc-air 1 M sample has been diluted to be consistent with the linearity range. The sample shows the peak of AA surrounded by other peaks representing the condensation and oxidation products of AA (see Fig. 9a).

The peaks appearing before AA, *i.e.* between 3.0 min and 3.76 min, are probably due to cleavage by-products of AA.

A further dilution does not allow one to separate the peaks better. The chromatogram (Fig. 9b) shows the main species, as well as the other degradation products.

The peak at 4.9 min belongs to DHA (UV spectrum close to that of AA). Comparing the chromatogram at 250 nm (Fig. 9b, gray) with the one at 280 nm (Fig. 9b, black), AA and DHA are the only products showing a lower intensity at 280 nm, as for AA-air sample.

The CaAsc-N_2 sample (Fig. 10) was extracted after N_2 cycling and was diluted under N_2 atmosphere to avoid contact with air. For a quantitative determination, calibration curves were created using AA and oxalic acid (OA).

The chromatogram in Fig. 10 is magnified to keep the intensity of the other products high enough to provide a tentative estimation of their quantity (Table 3). As for the most intense peaks (DP1 and DP2), their concentration has been approximatively evaluated using the same response factor as AA's. Oxalic acid appears at very low concentration, and its presence is likely due to the degradation of AA during the transfer of the solution. As to the nature of DP1 and DP2, it is possible to assume that DP2 is less polar than AA, with a polarity probably similar to that of DHA. On the opposite, DP1 is slightly more polar than AA but less than OA and might, therefore, be an intermediate degradation product.

In summary, HPLC measurements confirm the absence of oxalic acid as the final product of the AA degradation cascade in the absence of oxygen and carbon dioxide.

3.3. Single crystal X-ray on weddellite samples

Weddellite crystallizes in tetragonal *I*4/*m* space group (Sterling, 1965; Tazzoli and Domeneghetti, 1980). The main "building block" of the weddellite structure is the Ca-polyhedron, which forms a total of 8 bonds with O atoms, in particular 6 with O of the oxalate groups (four bonds with O1 and two bonds with O2) and 2 with O of H_2O molecules (OW1 and OW2). Each Ca-polyhedron shares the O1-O1 edge with two other equivalent polyhedra to form infinite chains along [001] direction;

Table ??3??
Main products, retention times and concentrations as measured on CaAsc-N_2.

	Retention time (min)	Starting concentration (mol/L)	Final concentration (mol/L)
AA	4.4	0.5	0.29
OA	2.9	–	2,52E−04
DP1	3.4	–	6,86E−04
DP2	8.2	–	1,25E−03

such chains are connected to each other *via* C_2O_4-H_2O-C_2O_4 complexes and the connection between C_2O_4 and H_2O is a hydrogen bond.

Rotation of Ca-polyhedra chains and H_2O-oxalate groups around the fourfold axis determines the formation of a channel along the *c* direction; the walls of the channel are formed by H_2O molecules OW1 and four of them are arranged in the plane 001, giving a regular square with OW1-OW1 edge equal to about 3.2 Å. At the center of the large channel, there are "zeolitic" water molecules that can be arranged in two crystallographically independent sites with partial occupancy (OW3 and OW31) (Fig. 11). Izatulina and coworkers (Izatulina et al., 2014) found a correlation between the amount of the zeolitic water and the unit cell *a* parameter ($x = 5.43 \times a - 66.80$, where *x* is the number of molecules p.f.u.); this correlation is in turn linked to OW1-OW1 distance in the large channel along c direction.

X-ray diffraction intensities were measured at room conditions on two crystals (CaOX-A-1 and G13–3) from as many syntheses.

In the case of the first investigated crystal (CaOX-A-1; crystal size 15 μm × 20 μm × 35 μm), cell parameter were refined using 493 reflections ($a = 12.3582(3)$ Å, $c = 7.3597(4)$ Å and $V = 1124.0(5)$ Å^3). Data collection and refinement details are reported in Tables SI3 and SI4 (see Supporting Information). Atomic position and anisotropic thermal parameters were refined for Ca, C and O sites; the H atom were refined with isotropic thermal parameters and the H_2O zeolitic water molecule was distributed on two different positions, aligned along [001] direction (OW3 and OW31). Main bond distances and electron contents (where refined) are shown in Table SI4 (Supporting Information) and exhibit a good agreement with the existing ones from literature.

Following Izatulina et al. (Izatulina et al., 2014), the *a* cell parameter suggests an amount of zeolitic water in the structure, as much as about 0.30 molecule p.f.u. The numbers of electrons ascribable to the symmetry independent OW30 and OW31 sites, from structure refinement, are 3.05 and 1.45e-, respectively. Taking into account that one has $10e^-$ per H_2O-molecule, one infers 0.31 and 0.14 H_2O-occupancy factors, at OW30 and OW31, respectively. In this light, the estimated total zeolitic water content, resulting from summing up OW30 and OW31 H_2O-occupancy factors, is as large as 0.45 H_2O molecule p.f.u.

The second crystal (G13–3; crystal size 13 μm × 15 μm × 20 μm) allowed X-ray diffraction data collections with fewer and less intense reflections than CaOX-A-1. However, the number of *unique* reflections is almost the same for either crystal (Table SI3, Supporting Information). The unit cell parameters were refined on the base of 125 reflections ($a = 12.378(4)$ Å, $c = 7.389(3)$ Å and $V = 1132.2(7)$ Å^3). Structural details were refined following the same strategy as CaOX-A-1, but the isotropic thermal parameters of H atoms were fixed to their average value from literature. Main bond distances and site electron contents are reported in Table SI4 (see Supporting Information). The zeolitic H_2O was localized in only one site (OW3); refinement results did not suggest the need to split the site into two different positions. Both electron refinement and Izatulina formula indicate a larger amount of zeolitic H_2O than that of the CaOX-A-1 crystal (0.55 and 0.41 molecules p.f.u. respectively). The OW1-OW1 distance of 3.302 Å is the longest reported in the

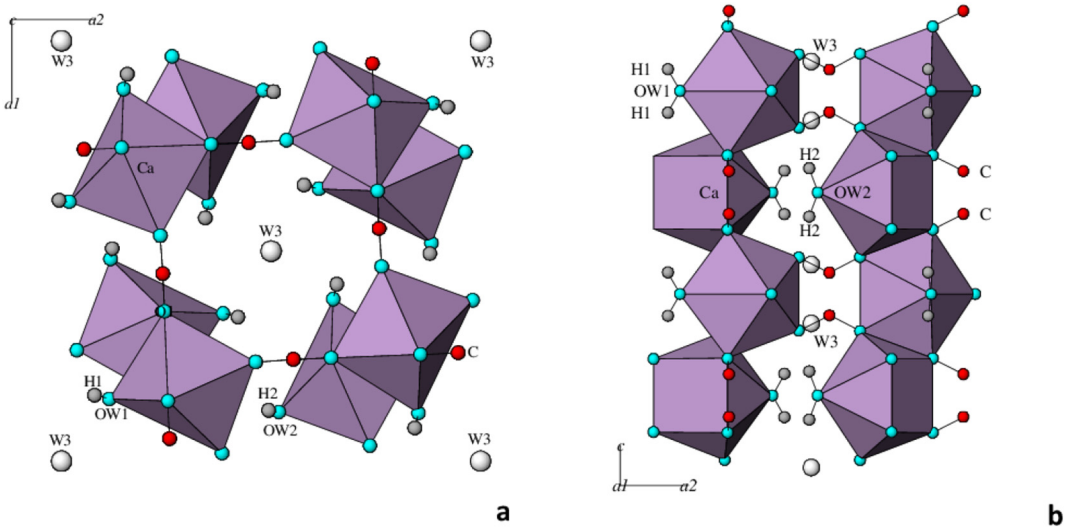

Fig. 11. a) Weddellite crystal structure along the c axis and b) along the a axis. (O: light blue; H: gray; Ca: purple; C: red; zeolitic H_2O: white).

literature so far (Izatulina et al., 2014, 2018) and also indicate a large amount of zeolitic water.

Altogether, CaOX-A-1 and G13-3 exhibit very similar crystal structures, as shown by Tables SI3 and SI4, and the differences seem mostly attributable to the guest H_2O molecules entering Ca-oxalate samples that form in a naturally H_2O-oversaturated environment.

4. Conclusions

In the present work, a direct and green method to convert C(IV) into C(III) and trap carbon dioxide into a stable crystalline structure other than a carbonate is discussed. The reaction has been validated, and its kinetics and trapping yield will be discussed in a further paper.

The conversion of carbon dioxide into oxalates doubles the capturing ratio ($CO_2/C_2O_4^{2-}$ 2:1) with respect to the traditional carbonation process (CO_2/CO_3^{2-} 1:1). Besides, the dissolution of the calcium oxalates does not directly yield carbon dioxide, as it occurs in the case of carbonates, thus meaning that should dissolution occur, CO_2 would not be straight released in the environment.

Calcium ascorbate (CaAsc) is a green and cost-sustainable reagent, widely used and studied in the food industry. Its application to our purposes leads to the capture and conversion of carbon dioxide *via* a green reaction. The ascorbic acid degradation cascade has been proven to have no or just feeble interference with the production of calcium oxalate from the reduction of carbon dioxide, and the products of the degradation of ascorbic acid are generally considered not harmful.

Under our experimental conditions, was precipitated almost selectively weddellite, a nearly insoluble crystal phase, with solubility lower than calcite, and stable in a wider pH range than carbonates. As X-ray single crystal diffraction experiments confirm, crystals precipitated from CaAsc solution are of high quality, which thing reflects on their stability, essential for storage purposes.

Although weddellite crystals obtained by different experimental setups show different morphological features, they exhibit stable flat (F) forms. Further works should be done on the possibility of direct the crystallization towards selected stable hydration states and morphologies characterized by low surface energies, to increase the stability of the precipitate under storage conditions and minimize the expected dehydration effect. Nevertheless, the dehydration driven phase transition towards the stable whewellite form of calcium oxalate does not affect the reliability of the method proposed.

The experiments show that the production of calcium oxalate from CO_2 can be described as a two-step process, following two main reactions: i) a red-ox reaction that involves the CaAsc solution, to act as the reductant triggering the conversion of CO_2 into $C_2O_4^{2-}$; ii) the nucleation of calcium oxalate. Given that the red-ox reaction appears to be the rate-determining step of the process, it should be boosted to decrease the system response time, for example acting upon temperature and pH, which are reported in the literature to be able to tune the reducing power of ascorbic acid.

Additionally, the reaction rate of the whole process has been found to be strongly dependent on the degree of subdivision of the CaAsc solution, *i.e.*, on the extent of the interface between the solution and CO_2. In fact, the reaction yield increases from 0.6 ppm/h for the B setup to a mean value of 12 ppm/h for the BD setup only increasing the reaction surface by introducing a partitioning pump into the solution pathway. The reaction yield could be increased explosively by decreasing the radius of the droplets to the micrometric size. It has been roughly evaluated that, for droplets with radius 2.5 μm, the BD setup yield with a reaction rate of 12 ppm/h will be increased by 42 k times.

In the light of these considerations, the experiments presented here represent a preliminary approach to further work devoted to the increase of the reaction yield by a fine dispersed solution in a gas (aerosol), tuning pH and temperature in order to prompt the rate-limiting step of the process.

CRediT authorship contribution statement

Linda Pastero: Conceptualization, Data curation, Formal analysis, Investigation, Methodology, Supervision, Validation, Visualization, Writing - original draft, Writing - review & editing. **Nadia Curetti:** Data curation, Formal analysis, Writing - original draft, Writing - review & editing. **Marco Aldo Ortenzi:** Data curation, Formal analysis. **Marco Schiavoni:** Data curation. **Enrico Destefanis:** Data curation. **Alessandro Pavese:** Funding acquisition, Supervision, Writing - original draft, Writing - review & editing.

Acknowledgements

The Authors would like to thank Professor Dino Aquilano for the fruitful discussion about PBC and face character of weddellite.

Funding

This work was supported by Università degli Studi di Torino, Turin, Italy.

Appendix A. Supplementary data

Supplementary data to this article can be found online at https://doi.org/10.1016/j.scitotenv.2019.02.114.

References

Amatore, C., Saveant, J.M., 1981. Mechanism and kinetic characteristics of the electrochemical reduction of carbon dioxide in media of low proton availability. J. Am. Chem. Soc. 103, 5021–5023. https://doi.org/10.1021/ja00407a008.

Angamuthu, R., Byers, P., Lutz, M., Spek, A.L., Bouwman, E., 2010. Electrocatalytic CO2 conversion to oxalate by a copper complex. Science 327, 313–315. https://doi.org/10.1126/science.1177981.

Aresta, M., Nobile, C.F., Albano, V.G., Forni, E., Manassero, M., 1975. New nickel–carbon dioxide complex: synthesis, properties, and crystallographic characterization of (carbon dioxide)-bis(tricyclohexylphosphine)nickel. J. Chem. Soc. Chem. Commun. 0, 636–637. https://doi.org/10.1039/C39750000636.

Bard, A.J., Parsons, R., Jordan, J., 1985. Standard Potentials in Aqueous Solution (Monographs in Electroanalytical Chemistry & Electrochemistry). Routledge https://doi.org/10.1201/9780203738764.

Bartlett, P.N., Wallace, E.N.K., 1999. The application of approximate analytical models in the development of modified electrodes for NADH oxidation. In: Compton, R.G., Hancock, G. (Gus) (Eds.), Comprehensive Chemical Kinetics. Applications of Kinetic Modelling Vol.37. Elsevier, Amsterdam; New York, pp. 35–89.

Benson, E.E., Kubiak, C.P., Sathrum, A.J., Smieja, J.M., 2009. Electrocatalytic and homogeneous approaches to conversion of CO $_2$ to liquid fuels. Chem. Soc. Rev. 38, 89–99. https://doi.org/10.1039/B804323J.

Bockris, J.O., Wass, J.C., 1989. The photoelectrocatalytic reduction of carbon dioxide. J. Electrochem. Soc. 136, 2521. https://doi.org/10.1149/1.2097455.

Bode, N., Rose, R.C., 1990. Spontaneous decay of oxidized ascorbic acid (dehydro-L-ascorbic acid) evaluated by ugh-pressure liquid chromatography w w TIME (minutes) TIME (minutes). Clin. Chem. 36, 1807–1809.

Borsook, H., Keighley, G., 1933. Oxidation-reduction potential of ascorbic acid (vitamin C). Proc. Natl. Acad. Sci. 19, 875–878. https://doi.org/10.1073/pnas.19.9.875.

Bretherton, T., Rodgers, A., 1998. Crystallization of calcium oxalate in minimally diluted urine. J. Cryst. Growth 192, 448–455. https://doi.org/10.1016/S0022-0248(98)00461-8.

Brown, P., Ackermann, D., Finlayson, B., 1989. Calcium oxalate dihydrate (weddellite) precipitation. J. Cryst. Growth 98, 285–292. https://doi.org/10.1016/0022-0248(89)90143-7.

Conti, C., Brambilla, L., Colombo, C., Dellasega, D., Gatta, G.D., Realini, M., Zerbi, G., 2010. Stability and transformation mechanism of weddellite nanocrystals studied by X-ray diffraction and infrared spectroscopy. Phys. Chem. Chem. Phys. 12, 14560–14566. https://doi.org/10.1039/c0cp00624f.

Conti, C., Casati, M., Colombo, C., Possenti, E., Realini, M., Gatta, G.D., Merlini, M., Brambilla, L., Zerbi, G., 2015. Synthesis of calcium oxalate trihydrate: new data by vibrational spectroscopy and synchrotron X-ray diffraction. Spectrochim. Acta A Mol. Biomol. Spectrosc. 150, 721–730. https://doi.org/10.1016/j.saa.2015.06.009.

Costentin, C., Robert, M., Savéant, J.-M., 2013. Catalysis of the electrochemical reduction of carbon dioxide. Chem. Soc. Rev. 42, 2423–2436. https://doi.org/10.1039/C2CS35360A.

Darensbourg, D.J., Rokicki, A., Darensbourg, M.Y., 1981. Facile reduction of carbon dioxide by anionic group 6B metal hydrides. Chemistry relevant to catalysis of the water-gas shift reaction. J. Am. Chem. Soc. 103, 3223–3224.

Daudon, M., 2015. Cristallurie. Nephrol. Ther. 11, 174–190. https://doi.org/10.1016/j.nephro.2015.03.003.

Daudon, M., Frochot, V., 2015. Crystalluria. Clin. Chem. Lab. Med. 53, S1479–S1487. https://doi.org/10.1515/cclm-2015-0860.

Finn, C., Schnittger, S., Yellowlees, L.J., Love, J.B., 2012. Molecular approaches to the electrochemical reduction of carbon dioxide. Chem. Commun. 48, 1392–1399. https://doi.org/10.1039/C1CC15393E.

Franchini-Angela, M., Aquilano, D., 1979. Growth morphology of weddellite CaC2O4 · 2x H2O. J. Cryst. Growth 47, 719–726. https://doi.org/10.1016/0022-0248(79)90017-4.

García-España, E., Gaviña, P., Latorre, J., Soriano, C., Verdejo, B., 2004. CO2Fixation by copper(II) complexes of a Terpyridinophane Aza receptor. J. Am. Chem. Soc. 126, 5082–5083. https://doi.org/10.1021/ja039577h.

Garvie, L.A.J., 2006. Decay of cacti and carbon cycling. Naturwissenschaften 93, 114–118. https://doi.org/10.1007/s00114-005-0069-7.

Gómez-Morales, J., Hernández- Hernández, Á., Sazaki, G., García-Ruiz, J.M., 2010. Nucleation and polymorphism of calcium carbonate by a vapor diffusion sitting drop crystallization technique. Cryst. Growth Des. 10, 963–969. https://doi.org/10.1021/cg901279t.

Graustein, W.C., Cromack, K., Sollins, P., 1977. Calcium oxalate: occurrence in soils and effect on nutrient and geochemical cycles. Science 198, 1252–1254. https://doi.org/10.1126/science.198.4323.1252.

Green, M.A., Fry, S.C., 2005. Vitamin C degradation in plant cells via enzymatic hydrolysis of 4-*O*-oxalyl-l-threonate. Nature 433, 83–87. https://doi.org/10.1038/nature03172.

Hartl, W.P., Klapper, H., Barbier, B., Ensikat, H.J., Dronskowski, R., Müller, P., Ostendorp, G., Tye, A., Bauer, R., Barthlott, W., 2007. Diversity of calcium oxalate crystals in Cactaceae. Can. J. Bot. 85, 501–517. https://doi.org/10.1139/B07-046.

Heijnen, W.M.M., Van Duijneveldt, F.B., 1984. The theoretical growth morphology of calcium oxalate dihydrate. J. Cryst. Growth 67, 324–336. https://doi.org/10.1016/0022-0248(84)90192-1.

Izatulina, A., Gurzhiy, V., Frank-Kamenetskaya, O., 2014. Weddellite from renal stones: structure refinement and dependence of crystal chemical features on H2O content. Am. Mineral. 99, 2–7. https://doi.org/10.2138/am.2014.4536.

Izatulina, A.R., Gurzhiy, V.V., Krzhizhanovskaya, M.G., Kuz'mina, M.A., Leoni, M., Frank-Kamenetskaya, O.V., 2018. Hydrated calcium oxalates: crystal structures, thermal stability, and phase evolution. Cryst. Growth Des. 18, 5465–5478. https://doi.org/10.1021/acs.cgd.8b00826.

Izumi, S., Shimakoshi, H., Abe, M., Hisaeda, Y., 2010. Photo-induced ring-expansion reactions mediated by B12-TiO2 hybrid catalyst. Dalton Trans. 39, 3302. https://doi.org/10.1039/b921802e.

Kortlever, R., Shen, J., Schouten, K.J.P., Calle-Vallejo, F., Koper, M.T.M., 2015. Catalysts and reaction pathways for the electrochemical reduction of carbon dioxide. J. Phys. Chem. Lett. 6, 4073–4082. https://doi.org/10.1021/acs.jpclett.5b01559.

Koshiishi, I., Mamura, Y., Imanari, T., 1998. Bicarbonate promotes a cleavage of lactone ring of dehydroascorbate. Biochim. Biophys. Acta, Gen. Subj. 1379, 257–263. https://doi.org/10.1016/S0304-4165(97)00106-2.

Kurata, T., Sakurai, Y., 1967. Degradation of L-ascorbic acid and mechanism of nonenzymic browning reaction. Agric. Biol. Chem. 31, 170–184. https://doi.org/10.1080/00021369.1967.10858792.

Kurata, T., Wakabayashi, H., Sakurai, Y., 1967. Degradation of L-ascorbic acid and mechanism of non-enzymic browning reaction. Agric. Biol. Chem. 31, 101–105. https://doi.org/10.1080/00021369.1967.10858773.

Kushi, Y., Nagao, H., Nishioka, T., Isobe, K., Tanaka, K., 1995. Remarkable decrease in overpotential of oxalate formation in electrochemical CO $_2$ reduction by a metal–sulfide cluster. J. Chem. Soc. Chem. Commun. 0, 1223–1224. https://doi.org/10.1039/C39950001223.

Lakshminarayanan, R., Kini, R.M., Valiyaveettil, S., 2002. Investigation of the role of ansocalcin in the biomineralization in goose eggshell matrix. Proc. Natl. Acad. Sci. U. S. A. 99, 5155–5159. https://doi.org/10.1073/pnas.072658899.

Latimer, W.M., 1952. The Oxidation States of the Elements and Their Potentials in Aqueous Solutions. Prentice-Hall chemistry series 1952. Prentice-Hall, New York.

Lide, D.R. (Ed.), 2003. CRC Handbook of Chemistry and Physics: A Ready-reference Book of Chemical and Physical Data, 84th ed. CRC Press, Boca Raton, FL.

Lovander, M.D., Lyon, J.D., Parr Iv, D.L., Wang, J., Parke, B., Leddy, J., 2018. Review—electrochemical properties of 13 vitamins: a critical review and assessment. J. Electrochem. Soc. 165, 18–49. https://doi.org/10.1149/2.1471714jes.

Markarian, S.A., Sargsyan, H.R., 2011. Electronic absorption spectra of ascorbic acid in water and water–dialkylsulfoxide mixtures. J. Appl. Spectrosc. 78, 6–10. https://doi.org/10.1007/s10812-011-9418-9.

Matsui, T., Kitagawa, Y., Okumura, M., Shigeta, Y., 2015. Accurate standard hydrogen electrode potential and applications to the redox potentials of vitamin C and NAD/NADH. J. Phys. Chem. A 119, 369–376. https://doi.org/10.1021/jp508308y.

Monje, P.V., Baran, E.J., 2002. Characterization of calcium oxalates generated as biominerals in cacti. Plant Physiol. 128, 707–713. https://doi.org/10.1104/pp.010630.

Notni, J., Schenk, S., Görls, H., Breitzke, H., Anders, E., 2008. Formation of a unique zinc carbamate by CO2 fixation: implications for the reactivity of tetra-azamacrocycle ligated Zn(II) complexes. Inorg. Chem. 47, 1382–1390. https://doi.org/10.1021/ic701899u.

Ouyang, J.-M., Zheng, H., Deng, S.-P., 2006. Simultaneous formation of calcium oxalate (mono-, di-, and trihydrate) induced by potassium tartrate in gelatinous system. J. Cryst. Growth 293, 118–123. https://doi.org/10.1016/J.JCRYSGRO.2006.05.008.

Paik, W., Andersen, T.N., Eyring, H., 1969. Kinetic studies of the electrolytic reduction of carbon dioxide on the mercury electrode. Electrochim. Acta 14, 1217–1232. https://doi.org/10.1016/0013-4686(69)87019-2.

Parsons, H.T., Fry, S.C., 2010. Reactive oxygen species-induced release of intracellular ascorbate in plant cell-suspension cultures and evidence for pulsing of net release rate. New Phytol. 187, 332–342. https://doi.org/10.1111/j.1469-8137.2010.03282.x.

Pastero, L., Aquilano, D., 2018. Calcium carbonate polymorphs growing in the presence of Sericin: a new composite mimicking the hierarchic structure of nacre. Crystals 8, 263. https://doi.org/10.3390/cryst8070263.

Qiao, J., Liu, Y., Hong, F., Zhang, J., 2014. A review of catalysts for the electroreduction of carbon dioxide to produce low-carbon fuels. Chem. Soc. Rev. 43, 631–675. https://doi.org/10.1039/C3CS60323G.

Qu, Y., Duan, X., 2013. Progress, challenge and perspective of heterogeneous photocatalysts. Chem. Soc. Rev. 42, 2568–2580. https://doi.org/10.1039/C2CS35355E.

Rosen, B.A., Salehi-Khojin, A., Thorson, M.R., Zhu, W., Whipple, D.T., Kenis, P.J.A., Masel, R.I., 2011. Ionic liquid-mediated selective conversion of CO2 to CO at low overpotentials. Science 334, 643–644. https://doi.org/10.1126/science.1209786 (80-.).

Savéant, J.-M., 2008. Molecular catalysis of electrochemical reactions. Mechanistic aspects. Chem. Rev. 108, 2348–2378. https://doi.org/10.1021/cr068079z.

Schneider, J., Jia, H., Muckerman, J.T., Fujita, E., 2012. Thermodynamics and kinetics of CO2, CO, and H+ binding to the metal centre of CO2 reduction catalysts. Chem. Soc. Rev. 41, 2036–2051. https://doi.org/10.1039/C1CS15278E.

Seshadri, G., Lin, C., Bocarsly, A.B., 1994. A new homogeneous electrocatalyst for the reduction of carbon dioxide to methanol at low overpotential. J. Electroanal. Chem. 372, 145–150. https://doi.org/10.1016/0022-0728(94)03300-5.

Shah, K.J.., Pan, A.-Y., Gandhi, V., Chiang, P.-C., 2018. Photo-electrochemical reduction of CO2 to solar fuel: A review. Photocatalytic Nanomaterials for Environmental Applications. Vol. 27. Materials Research Foundations. Materials Research Forum LLC, pp. 211–235.

Sterling, C., 1965. Crystal structure analysis of weddellite, CaC2O4.(2+x)H2O. Acta Crystallogr. 18, 917–921. https://doi.org/10.1107/S0365110X65002219.

Tazzoli, V., Domeneghetti, C., 1980. The crystal structures of whewellite and weddellite; re-examination and comparison. Am. Mineral. 65, 327–334.

Tryk, D., Yamamoto, T., Kokubun, M., Hirota, K., Hashimoto, K., Okawa, M., Fujistima, A., 2001. Recent developments in electrochemical and photoelectrochemical CO2

reduction: involvement of the (CO2)(2)(.-) dimer radical anion. Appl. Organomet. Chem. 15, 113–120.
van Albada, G.A., Mutikainen, I., Roubeau, O., Turpeinen, U., Reedijk, J., 2002. Ferromagnetic trinuclear carbonato-bridged and tetranuclear hydroxo-bridged Cu(II) compounds with 4,4′-dimethyl-2,2′-bipyridine as ligand. X-ray structure, spectroscopy and magnetism. Inorg. Chim. Acta 331, 208–215. https://doi.org/10.1016/S0020-1693(01)00808-8.
Verdejo, B., Aguilar, J., García-España, E., Gaviña, P., Latorre, J., Soriano, C., Llinares, J.M., Doménech, A., 2006. CO2 fixation by Cu2+ and Zn2+ complexes of a terpyridinophane aza receptor. Crystal structures of Cu2+ complexes, pH-metric, spectroscopic, and electrochemical studies. Inorg. Chem. 45, 3803–3815. https://doi.org/10.1021/ic060278d.
Whipple, D.T., Kenis, P.J.A., 2010. Prospects of CO 2 utilization via direct heterogeneous electrochemical reduction. J. Phys. Chem. Lett. 1, 3451–3458. https://doi.org/10.1021/jz1012627.
Youngme, S., Chaichit, N., Kongsaeree, P., van Albada, G.A., Reedijk, J., 2001. Synthesis, structure, spectroscopy, and magnetism of two new dinuclear carbonato-bridged Cu(II) complexes. Inorg. Chim. Acta 324, 232–240. https://doi.org/10.1016/S0020-1693(01)00610-7.
Zhang, J., Yang, H., Shen, G., Cheng, P., Zhang, J., Guo, S., 2010. Reduction of graphene oxide via L-ascorbic acid. Chem. Commun. 46, 1112–1114. https://doi.org/10.1039/B917705A.